Magnetic Reversals in a Simple Model of Magnetohydrodynamics

Roberto Benzi[1] and Jean-François Pinton[2]

[1]*Dipartimento di Fisica and INFN, Università "Tor Vergata," Via della Ricerca Scientifica 1, I-00133 Roma, Italy*
[2]*Laboratoire de Physique, CNRS and École Normale Supérieure de Lyon, 46 allée d'Italie, F69007 Lyon, France*
(Received 1 May 2009; published 8 July 2010)

We study a simple magnetohydrodynamical approach in which hydrodynamics and MHD turbulence are coupled in a shell model, with given dynamo constraints in the large scales. We consider the case of a low Prandtl number fluid for which the inertial range of the velocity field is much wider than that of the magnetic field. Random reversals of the magnetic field are observed and it shown that the magnetic field has a nontrivial evolution—linked to the nature of the hydrodynamics turbulence.

DOI: 10.1103/PhysRevLett.105.024501 PACS numbers: 47.27.Ak, 91.25.Cw

The question of transitions between statistical solutions is central to the behavior of many out-of-equilibrium systems in physics and geophysics [1–4]. As one particular example addressed here, we note that natural dynamos are intrinsically dynamical. Formally, the coupled set of momentum and induction equations is invariant under the transform $(\mathbf{u}, \mathbf{B}) \rightarrow (\mathbf{u}, -\mathbf{B})$ so that states with opposite polarities can be generated from the same velocity field ($\mathbf{u}$ and $\mathbf{B}$ are, respectively, the velocity and magnetic fields). In the case of the geodynamo, polarity switches are called reversals [5] and occur at very irregular time intervals [6]. Such reversals have been observed recently in laboratory experiments using liquid metals, in arrangements where the dynamo cycle is either favored artificially [7] or stems entirely from the fluid motions [4,8]. In these laboratory experiments, as also presumably in Earth's core, the ratio of the magnetic diffusivity to the viscosity of the fluid (magnetic Prandtl number P_M) is quite small. As a result, the kinetic Reynolds number R_V of the flow is very high because its magnetic Reynolds number $R_M = R_V P_M$ needs to be large enough so that the stretching of magnetic field lines balances the Joule dissipation. Hence, the dynamo process develops over a turbulent background, and in this context it is often considered as a problem of "bifurcation in the presence of noise." For the dynamo instability, the effect of noise enters both additively and multiplicatively, a situation for which a complete theory is not currently available. Some specific features have been ascribed to its onset (e.g., bifurcation via an on-off scenario [9]) and to its dynamics [10]. Turbulence also implies that processes occur over an extended range of scales; however, in a low magnetic Prandtl number fluid the hydrodynamic range of scales is much wider than the magnetic one. In laboratory experiments, the induction processes that participate in the dynamo cycle involve the action of large scale velocity gradients [4,11,12], with possible contributions of velocity fluctuations at small scales [13–15].

Building upon the above observations, we propose here a simple model which incorporates hydromagnetic fluctuations (as opposed to "noise") in a dynamo instability. Our goal here is not to derive a low dimensional model from the interaction of selected modes (see, for instance, [16] and references therein) but to assume the existence of such large scale symmetry-breaking features and to investigate the effects of turbulence fluctuations onto the dynamics of reversals. The models stems from the approach introduced in [17] for the hydrodynamic studies.

We consider an "energy cascade" model, i.e., a shell model aimed at reproducing a few of the relevant characteristic features of the statistical properties of the Navier-Stokes equations [18]. In a shell model, the basic variables describing the "velocity field" at scale $r_n = 2^{-n} r_0 \equiv k_n^{-1}$ is a complex number u_n satisfying a suitable set of nonlinear equations (here $r_0 = 2$). There are many versions of shell models which have been introduced in literature. Here we choose the one referred to as *Sabra* shell model. Let us remark that the statistical properties of intermittent fluctuations, computed using either shell variables or the instantaneous rate of energy dissipation, are in close qualitative and quantitative agreement with those measured in laboratory experiments, for homogeneous and isotropic turbulence [18]. The MHD shell model—introduced in [19]—allows a description of turbulence at low magnetic Prandtl number since the steps of both cascades can be freely adjusted [20,21]. Although geometrical features are lost, this is a clear advantage over 3D simulations [22,23]. We consider here a formulation extended from the Sabra hydrodynamic shell model:

$$\frac{du_n}{dt} = \frac{i}{3}[\Phi_n(u,u) - \Phi_n(B,B)] - \nu k_n^2 u_n + f_n, \quad (1)$$

$$\frac{dB_n}{dt} = \frac{i}{3}[\Phi_n(u,B) - \Phi_n(B,u)] - \nu_m k_n^2 B_n, \quad (2)$$

where $n = 1, 2, \ldots$ and

$$\begin{aligned}\Phi_n(u,w) = {} & k_{n+1}[(1+\delta)u_{n+2}w_{n+1}^* + (2-\delta)u_{n+1}^* w_{n+2}] \\ & + k_n[(1-2\delta)u_{n-1}^* w_{n+1} - (1+\delta)u_{n+1} w_{n-1}^*] \\ & + k_{n-1}[(2-\delta)u_{n-1}w_{n-2} + (1-2\delta)u_{n-2}w_{n-1}],\end{aligned} \quad (3)$$

for which, following [17], we chose $\delta = -0.4$. For this value of δ, the Sabra model is known to show statistical properties (i.e., anomalous scaling) close to the ones observed in homogenous and isotropic turbulence. The model, without forcing and dissipation, conserves the kinetic energy $E_V = \Sigma_n |u_n|^2$, the magnetic energy $E_B = \Sigma_n |B_n|^2$, and the cross-helicity $\mathrm{Re}(\Sigma_n u_n B_n^*)$. In the same limit, the model has a $U(1)$ symmetry corresponding to a phase change $\exp(i\theta)$ in both complex variables u_n and B_n. The quantity $\Phi_n(v, w)$ is the shell model version of the transport term $\vec{u}\nabla\vec{w}$. The forcing term f_n is given by $f_n \equiv S_{1n} f_0 / u_1^*$; i.e., we force injection in the large scale with a constant power. We want to introduce in Eq. (2) an extra (large scale) term aimed at producing two statistically stationary equilibrium solutions for the magnetic field. For this purpose, we add to the right-hand side of (2) an extra term $M_2(B_2)$; namely, for $n = 2$, Eq. (2) becomes

$$\frac{dB_2}{dt} = F_2(u, B) - M_2(B_2) - \nu_m k_2^2 B_2, \quad (4)$$

where $F_2(u, B)$ is a shorthand notation for $i/3[\Phi_2(u, B) - \Phi_2(B, u)]$. The term $M_2(B_2)$ is chosen with two requirements: (1) it must break the $U(1)$ symmetry, and (2) it must introduce a large scale dissipation needed to equilibrate the large scale magnetic field production. There are many possible ways to satisfy these two requirements. Here we simply choose $M_2(B_2) = a_m B_2^3$. We argue, see the discussion at the end of this Letter, that the two requirements are a necessary condition to observe large scale equilibration. From a physical point of view, symmetry breaking also occurs in real dynamos since the magnetic field is directed in one preferential direction which changes sign during a reversal. Thus symmetry breaking is a generic feature which we introduce in our model by prescribing some large scale geometrical constrain. On the other hand, large scale dissipation must be responsible for the equilibration mechanism of the large scale field. The choice of a nonlinear equilibration is made here to highlight the existence of a nonlinear center manifold for the large scale dynamics [24]. In other words, Eq. (4) with $M_2(B_2) = a_m B_2^3$ is supposed to describe the "normal form" dynamics of the large scale magnetic field. Note that our assumption on M_2 does not necessarily imply a time scale separation between the characteristic time scale of B_2 and the magnetic turbulent field. Finally, since the system has an inverse cascade of helicity [19], we set $B_1 = 0$ as a boundary condition at large scale in order to prevent nonstationary behavior.

The free parameters of the model are the power input f_0, the magnetic viscosity ν_m, and the saturation parameters a_m. Our numerical simulations have been computed with $n = 1, 2, \ldots, 25$. Actually, the parameter f_0 could be eliminated by a suitable rescaling of the velocity field. We shall keep it fixed to $f_0 = 1 - i$. In Fig. 1 we show the amplitude of $\langle |B_2| \rangle$ and the magnetic energy $E_B \equiv \langle \Sigma_n |B_n|^2 \rangle$ as a function of ν_m for $\nu = 10^{-7}$, where the symbol $\langle \cdots \rangle$ stands for time average. In this system, a possible estimate of Reynolds numbers is $R_V = \sqrt{\langle E_V \rangle}/k_2 \nu = \sqrt{\langle E_V \rangle} r_0 / 4\nu$ and $R_M = \sqrt{\langle E_V \rangle} r_0 / 4\nu_m$; in the runs shown, $\langle E_V \rangle \sim 0.3$, this yields $R_V \sim 1.5 \times 10^6$ and $R_M \sim 0.15/\nu_m$.

For very large ν_m, the magnetic field does not grow. Then, for ν_m greater than some critical value, $\langle B_2 \rangle$, as well as E_B, increases for decreasing ν_m. Eventually, $\langle |B_2| \rangle$ saturates at a given value while E_B still increases, showing that for ν_m small enough a fully developed spectrum of B_n is achieved. This type of behavior is in agreement with previous studies of Taylor-Green flows [25,26], $s_2 t_2$ flows in a sphere [27], or MHD shell models [28]. In the top inset of Fig. 1 we show the magnetic and energy spectrum for $\nu_m = 10^{-3}$. Finally, in the lower inset we plot the magnetic dissipation $\epsilon_B = \nu_m \Sigma_n k_n^2 \langle |B_n|^2 \rangle$ and the large scale dissipation due to M_n. Note that at the dynamo threshold we observe a sudden bump in the magnetic dissipation which decreases for decreasing ν_n. At relatively small ν_m, the magnetic dissipation becomes constant and quite close to the large scale dissipation.

We can reasonably predict the behavior of $\langle |B_2|^2 \rangle$ as a function of ν_m by the following argument. The onset of dynamo implies that there exists a net flux of energy from the velocity field to the magnetic field. At the largest scale, the magnetic field B_2 is forced by the velocity field due to the terms $F_2(u, B)$. The quantity $A \equiv \mathcal{R}[F_2(u, B) B_2^*]$ is the energy pumping due to the velocity field which is independent of B_2 and a_m. Thus, from Eq. (4) we can obtain

$$\frac{1}{2} \frac{d|B_2|^2}{dt} = A - a_m |B_2|^2 (B_{2r}^2 - B_{2i}^2) - \nu_m k_2^2 |B_2|^2, \quad (5)$$

where B_{2r} and B_{2i} are the real and imaginary part of B_2. For large ν_m, the amplitude of B_2 is small and the symmetry-breaking term proportional to a_m is negligible. Under this condition, and with the boundary condition constraints, we expect from (5) or (7) that the behavior of B_2 is periodic, as it has been observed in the numerical simulations. On the other hand, for relatively small ν_m, the nonlinear equili-

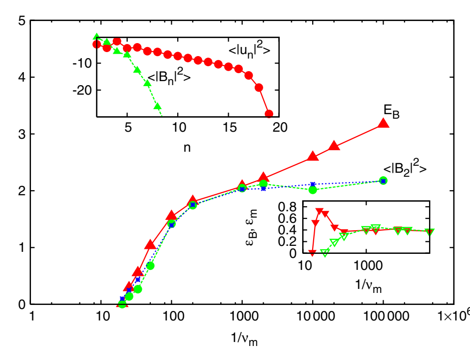

FIG. 1 (color online). Main figure: The behavior of $\langle E_B \rangle$ (red triangles) and $\langle |B_2|^2 \rangle$ (green circles) as a function of ν_m for fixed value of $\nu = 10^{-7}$. The dotted blue line is the solution of (5). Upper inset: Energy spectra for B_n (green triangles) and u_n (red circles) for the case $\nu_m = 0.001$. Lower inset: The amount of magnetic dissipation (solid red triangles) $\epsilon_B = \langle \Sigma_n \nu_m k_n^2 |B_n|^2 \rangle$ and the dissipation due to the large scale term $\epsilon_m = a_m \langle |B_2|^2 (B_{2r}^2 - B_{2i}^2) \rangle$ (open green triangles).

bration breaks the $U(1)$ symmetry and B_{2i} becomes rather small and statistically stationary solutions can be observed with $B_{2r}^2 = \sqrt{A/a_m}$. Computing A from the numerical simulations, we can use (5) to predict how $\langle |B_2|^2 \rangle$ depends on ν_m. The result is shown in Fig. 1 by the dotted blue line with rather good agreement.

We are interested in studying the behavior of the magnetic reversal, if any, as a function of ν_m and, in particular, in the region where $|B_2|$ saturates, i.e., it becomes independent of ν_m. In Fig. 2, we show three different time series of the $B_{2r} = \mathrm{Re}(B_2)$ as a function of time for three different, relatively large, values of the magnetic diffusivity. The figure highlights the two major items discussed in this Letter, namely, the observation of reversals between the two possible large scale equilibria and the dramatic increase of the time delay between reversals for increasing ν_m values. Note that this long time scale, as observed in the upper panel of Fig. 2, is much longer than the characteristic time scale of B_2 near one of the two equilibrium states. The system spontaneously develops a significant time scale separation, for which given polarity is maintained for times much longer than the magnetic diffusion time. In Fig. 3 we show the average persistence time (i.e., time between reversals) as a function of ν_m. More precisely, let us define t_n as the times at which $B_2(t_n) = 0$ and B_2 has opposite sign before and after t_n. Then the persistence time is defined as $\tau_n \equiv t_n - t_{n-1}$, while the average persistence time τ is defined as the average of τ_n. In order to obtain a significant value of τ, we performed rather long numerical simulations (from 10^3 to 10^4 longer than the time series shown in Fig. 2).

Figure 3 clearly shows that for large ν_m, τ becomes extremely large (note that the figure is in log-log scale). Thus, even if neither $\langle |B_2|^2 \rangle$ nor ϵ_d depend on ν_m, the effect of magnetic diffusivity is crucial for determining the average persistence time. For each numerical simulation shown in Fig. 3, we computed the average persistence time τ and its error bar (see inset). In order to develop a theoretical framework aimed at understanding the result shown in Fig. 3, we assume, in the region where $\langle |B_2|^2 \rangle$ is independent of ν_m, that $B_{2i} \sim 0$ and that the term $F_2(u, B)$ can be divided into an average forcing term proportional to B_{2r} and a fluctuating part

$$F_2(u, B) = \beta B_2 + \phi', \tag{6}$$

where β depends on f_0 and ϕ' is supposed to be uncorrelated with the dynamics of B_2, i.e., $\langle [\phi' B_2^*] \rangle = 0$. Note that in the context of the mean-field approach to MHD, the first term βB_2 would correspond to an "alpha effect." Using (6) we can rewrite the equations for B_2 as follows:

$$\frac{dB_2}{dt} = \beta B_2 - a_m B_2^3 + \phi', \tag{7}$$

where we neglect the dissipative term since $\beta \gg \nu_m k_2^2$ in the region of interest. Equation (7) must be considered an effective equation describing the dynamics of the magnetic field B_2 and its reversals, and the fluctuations ϕ' incorporate the turbulent fluctuations from the velocity and magnetic field turbulent cascades. It is the effect of ϕ' that makes the system "jump" between the two statistically stationary states. Using (5) we can obtain $\beta = \sqrt{A a_m}$ while the two statistical stationary states can be estimated as $\pm B_0$, $B_0^2 = \beta / a_m$. The effective equation (7) is a stochastically differential equation. By using large deviation theory [29] applied to stochastic differential equations, we can predict τ to be

$$\tau \sim \exp\left(\frac{\beta^2}{a_m \sigma}\right) = \exp\left(\frac{A}{\sigma}\right), \tag{8}$$

where σ is the variance of the noise ϕ' acting on the system. Let us note that A and σ must have the same dimension, namely, $[B]^2/\mathrm{time}$. Thus, we write σ as $\sigma = Af$,

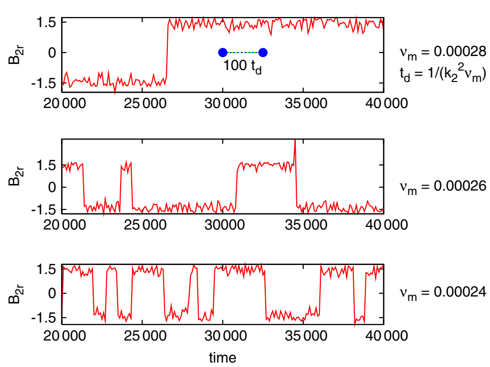

FIG. 2 (color online). Time behavior of B_{2r} for three different values of ν_m (displayed on the right-hand side) and constant ν. The short blue segment in the upper panel shows $100 t_d$, where t_d is the dissipative time scale computed as $t_d = 1/(k_2^2 \nu_m)$. One time unit in the figure corresponds to the large scale eddy turnover time $1/(k_1 |u_1|)$. Numerical simulations have run for much longer than the time intervals shown here—in the complete time series there is no asymmetry between the $\pm B_2$ states.

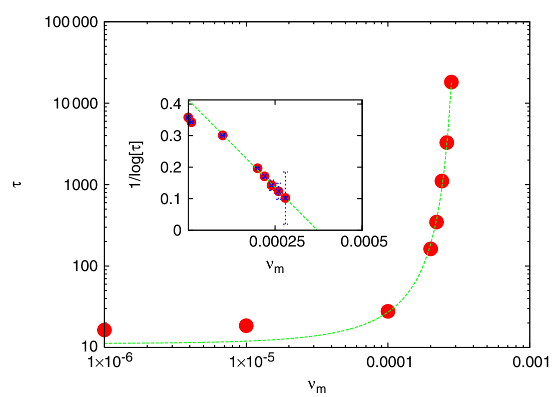

FIG. 3 (color online). Average persistence time τ as a function of the magnetic viscosity ν_m for $a_m = 0.1$ and $\nu = 10^{-7}$. The dotted green line corresponds to the fit given by Eq. (9). In the inset we plot $1/\ln(\tau)$ and its error bars (computed from the standard deviation) versus ν_m to highlight the linear behavior predicted by (9). Note that the error bars are smaller than the symbol size except for the very last point

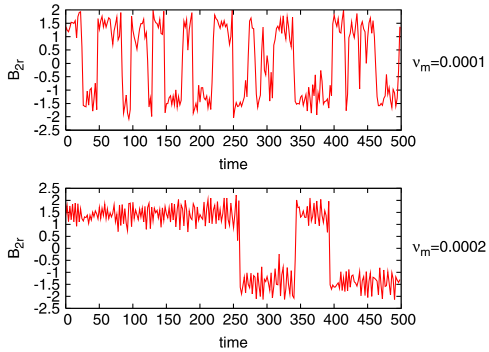

FIG. 4 (color online). Time behavior of B_{2r} for two different values of ν_m (displayed on the right) obtained by using a linear large scale equilibration $-\gamma B_2$ ($\gamma = 0.13$) and by imposing $B_{2i} = 0$. Note that although large scale equilibration is achieved by a linear damping on the magnetic field, B_{2r} shows quite well-defined statistical equilibria due to the symmetry-breaking constraint $B_{2i} = 0$.

where f is a function of the relevant dimensionless variables. In our problem the dimensionless numbers expected to play a role for the dynamical behavior of the magnetic field are the Reynolds number R_V, the magnetic Reynolds number R_M (or equivalently the magnetic Prandtl number P_M), and the quantity $R_m = \sqrt{Aa_m/(\nu_m^2 k_2^4)}$, which is an effective Reynolds number, corresponding to the efficiency of energy transfers from the velocity field to the magnetic field at large scale. Given the fact that we operate at constant power input and $R_V = \text{const}$, we expect f to be a function of (R_m, R_M) only and we also expect the effective magnetic Reynolds number to be proportional to the integral one ($R_m \propto R_M$). We then show below that a very good description of our numerical results is obtained using the lowest order approximation $f(R_m, R_M) = R_M^* - R_M$, where R_M^* is a critical magnetic Reynolds number below which reversals are not observed. This choice leads to $\sigma = A(\nu_m^* - \nu_m)/uL$ and finally to

$$\tau \sim \exp\left(\frac{C}{\nu_m^* - \nu_m}\right), \quad (9)$$

where C is a constant independent of ν_m. This functional form is displayed in Fig. 3; it agrees remarkably with the observed numerical values of τ for a rather large range. In the inset of Fig. 3 we show $1/\log(\tau)$ as a function of ν_m to highlight the linear behavior predicted by Eq. (9). The physical statement represented by (9) is that the average persistence time should show a critical slowing down for relatively large ν_m. In other words, we expect that fluctuations around the statistical equilibria increase as R_M increases. The increase of fluctuations may not be monotonic for very large R_M, which explains why we are not able to fit the entire range of ν_m shown in Fig. 3.

Finally, we comment on the choice of a nonlinear term in Eq. (4). Actually, we can avoid nonlinear equilibration to obtain the same (qualitative) results. In Fig. 4 we show two cases obtained with $M_2(B_2) = -\gamma B_2$ with the constraints $B_{2i} = 0$ and $\gamma = 0.13$. The equilibration mechanism is therefore linear while the symmetry breaking is obtained by the constraint $B_{2i} = 0$. Thus the two requirements, large scale dissipation and symmetry breaking, are satisfied. Figure 4 shows that statistical equilibria can be observed independent of nonlinear mechanism. Moreover, by changing the magnetic diffusivity, we can still observe a rather large difference in the average persistence time. We argue that this effect is independent of the particular choice of the equilibration mechanism since it is dictated by dimensional analysis and large deviation theory.

We thank Stephan Fauve for interesting discussions.

[1] E. R. Weeks *et al.*, Science **278**, 1598 (1997); A. J. Majda *et al.*, Proc. Natl. Acad. Sci. U.S.A. **103**, 8309 (2006).

[2] F. H. Busse, *Theories of Turbulence*, CISM Courses and Lectures Vol. 442 (Springer, Wien, 2002), p. 77.

[3] R. Verzicco and R. Camussi, J. Fluid Mech. **383**, 55 (1999); **477**, 19 (2003); F. Chillá *et al.*, Eur. Phys. J. B **40**, 223 (2004); R. J. A. M. Stevens *et al.*, Phys. Rev. Lett. **103**, 024503 (2009).

[4] R. Monchaux *et al.*, Phys. Rev. Lett. **98**, 044502 (2007).

[5] *Magnetohydrodynamics and the Earth's Core: Selected Works of Paul Roberts*, edited by A. M. Soward (CRC Press, London, 2003).

[6] R. T. Merrill, M. W. McElhinny, and P. L. McFadden, *The Magnetic Field of the Earth, Paleomagnetism, the Core and the Deep Mantle* (Academic, London, 1996).

[7] M. Bourgoin *et al.*, New J. Phys. **8**, 329 (2006).

[8] M. Berhanu *et al.*, Europhys. Lett. **77**, 59001 (2007).

[9] D. Sweet *et al.*, Phys. Rev. E **63**, 066211 (2001).

[10] P. Hoyng, M. A. J. H. Ossendrijver, and D. Schmitt, Geophys. Astrophys. Fluid Dyn. **94**, 263 (2001).

[11] A. Gailitis *et al.*, Phys. Rev. Lett. **86**, 3024 (2001).

[12] R. Stieglitz and U. Müller, Phys. Fluids **13**, 561 (2001).

[13] R. Stepanov *et al.*, Phys. Rev. E **73**, 046310 (2006).

[14] E. J. Spence *et al.*, Phys. Rev. Lett. **98**, 164503 (2007).

[15] S. A. Denisov *et al.*, JETP Lett. **88**, 167 (2008).

[16] F. Petrelis and S. Fauve, J. Phys. Condens. Matter **20**, 494203 (2008).

[17] R. Benzi, Phys. Rev. Lett. **95**, 024502 (2005).

[18] L. Biferale, Annu. Rev. Fluid Mech. **35**, 441 (2003).

[19] P. Frick and D. Sokoloff, Phys. Rev. E **57**, 4155 (1998).

[20] R. Stepanov and P. Plunian, J. Turbul. **7**, 1 (2006).

[21] F. Plunian and R. Stepanov, New J. Phys. **9**, 294 (2007).

[22] Y. Ponty, H. Politano, and J. F. Pinton, Phys. Rev. Lett. **92**, 144503 (2004).

[23] J. Baerenzung *et al.*, Phys. Rev. E **78**, 026310 (2008).

[24] L. Arnold, *Random Dynamical Systems*, Lecture Notes in Mathematics Vol. 1609 (Springer, Berlin, 1995).

[25] Y. Ponty *et al.*, Phys. Rev. Lett. **94**, 164502 (2005).

[26] J-P. Laval *et al.*, Phys. Rev. Lett. **96**, 204503 (2006).

[27] R. A. Bayliss *et al.*, Phys. Rev. E **75**, 026303 (2007).

[28] P. Frick, R. Stepanov, and D. Sokoloff, Phys. Rev. E **74**, 066310 (2006).

[29] S. R. S. Varadhan, Ann. Probab. **36**, 397 (2008); D. Ludwig, SIAM Rev. **17**, 605 (1975).